Defence Science Journal, Vol. 52, No. 4, October 2002, pp. 375-383

Analysis of Orthogonal Cutting of Aluminium-based Composites

P. Ravinder Reddy and A.A. Sriramakrishna

Chaitanya Bharathi Institute of Technology, Hyderabad – 500 075

ABSTRACT

A turning test on aluminium-based metal-matrix composites (MMCs) (aluminium-30% silicon carbide) was performed with K-20 carbide tool material and wear patterns and the wear land growth rates were analysed to evaluate the wear characteristics and to classify the relationship between the physical (mechanical) properties and the flank wear of cutting tools. The study was also extended to the machining aspects and the width of cuts on MMCs and the influence of various cutting parameters. The experiments were conducted to measure the temperature along the cutting tool edge using thermocouple at various cutting speeds, and depth of cuts, keeping the feed rate constant while turning with K-20 carbide cutting tool. The finite-element method was used to simulate the orthogonal cutting of aluminium-based MMCs. The heat generation at the chip-tool interface, frictional heat generation at the tool flank, and the heat generation at the work tool interface were calculated analytically and imposed as boundary conditions. The analysis of the steady-state heat transfer was carried out and the temperature distribution at cutting edge, shear zone, and interface regions have been reported.

Keywords: Metal-matrix composites, bonding material wear, aluminium-based composites, composite machining, orthogonal cutting, machining, turning test, wear pattern, wear land growth, wear characteristics, cutting tools, flank wear

1. INTRODUCTION

The metal-matrix composites(MMCs)generally consist of an alloy (2124 aluminium alloy) and a reinforcement (silicon carbide) material. The aluminium alloy, which is soft, binds the particles of silicon carbide. The main function of bonding material is to transfer and distribute the load to the reinforcement. In a conventional machining, a surface layer of the material is removed by a wedge-shaped tool. There is plastic deformation of the workpiece material, ahead of the cutting edge, due to the entry of the tool edge into the workpiece material and its subsequent shearing. The machining of composites significantly differs from metal machining in some respects. The fibres are laid in parallel, anti-parallel, and normal to the tool movement. In composite machining, three different mechanisms operate. These are micro-ploughing, micro-cutting, and micro-cracking. The hardened tool wedge enters the soft matrix and removes the material by abrasion. When cutting tool wedge enters the workpiece, a combination of the above mechanisms, i.e., plastic deformation, shearing, and rupturing may take place. The mechanism of chip formation also differs with the fibre angle in reference to the cutting direction. At zero fibre angle, cracking takes place in the direction of the fibre and at 90° fibre angle, block chips are pushed out to produce discontinuous chips, while shearing is suppressed by the fibres. Further, the machining of these composites are to be studied to know the mechanism of chip removal, the tool life, and the influence of cutting parameters. For a particular set of contacting materials, wear mechanism

Received 02 September 2002

maps have been used to identify the ranges of normal pressure and velocity that result in a particular wear mechanism. Cutting tool wear research has established similar maps for feed rate, which is related to pressure for a given engagement condition and velocity[1]. The crater wear condition with diffusion wear being the dominant mechanism[2]. Power, spindle torque, and force components on the tool are useful measurements[3]. Acoustic emission sensors are also proving to be of value[4-5] and the tool-life models are suggested by Zdeblick[6], *et al.* Measuring the performance of cutting tool materials and geometries over a broad range of materials and conditions is crucial to design improvement. Modern machining methods require cutting tools to be more versatile to handle a wide range of operations in an effort to reduce inventories and tool change time. A wide variety of machine tests are being regularly conducted to meet this goal and to understand the phenomena associated with machining. These tests encompass workpiece materials, cutting tools, and the cutting operations and their characterisation[7-13]. To understand the composite machining operations, it is necessary to understand the cutting action that occurs in the composites. This involves an analysis of the chip formation machinists, of the formation of the forces, and deformations developed in the material, rise in temperature which occur during machining. The present investigation aims to simulate the orthogonal cutting of MMCs using finite-element method.

2. EXPERIMENTAL EQUIPMENT/PROCEDURE

In this method, high speed HMT lathe (1450 mm x 800 mm x 5.5 kW) is used. The tested workpiece material is the aluminium composite (aluminium fibre and silicon carbide matrix) with a diameter of 60 mm, having a length of 225 mm, and volume fraction of 70 per cent. The tested tool tips are square inserts (12.7 mm and 12.7 mm x 4.7 mm, SNP-432-type) with tool geometry of 0.5°, 0.5°, 5°, 5°, 15°, 0.8 mm which are set in a standard tool holder. The material of the tool tip is K-20 carbide tool with 94 per cent WC and 6 per cent cobalt.

The cutting conditions are as follows:

A depth of cut (1 mm) and feed rate (0.1mm/rev) remain constant throughout in all the tests, several spindle speeds (i.e., cutting speeds) are chosen. The cutting fluid is used for washing-off the chips. The flank wear lands of tested tools were measured with Olympus's and the nose wear also measured by Toko Seimitsu's Surfcom 2B surface meter. The workpiece cutting edges were observed by Hitachi-Akashi's MSM-2 scanning electron microscope.

2.1 Experimental Setup for Temperature Measurement

The experiment is based on the fact that an electromotive force is generated at the interface of two dissimilar metals when the temperature of the interface changes. Experiments were conducted on MMC material of 60 mm diameter, specific gravity 1.7, and volume fraction 70 per cent, and K-20 carbide tool with a composition of 94 per cent WC and 6 per cent cobalt was selected as the cutting tool. A general turning experiment was taken as the basis for the measurement of temperature distribution on the cutting tool during machining. These experiments were conducted on a HMT lathe. A thermocouple was used to measure the temperatures at three different points on the cutting tool. A thermocouple setup and filter circuit is shown in Figs 1 and 2, respectively. A filter circuit

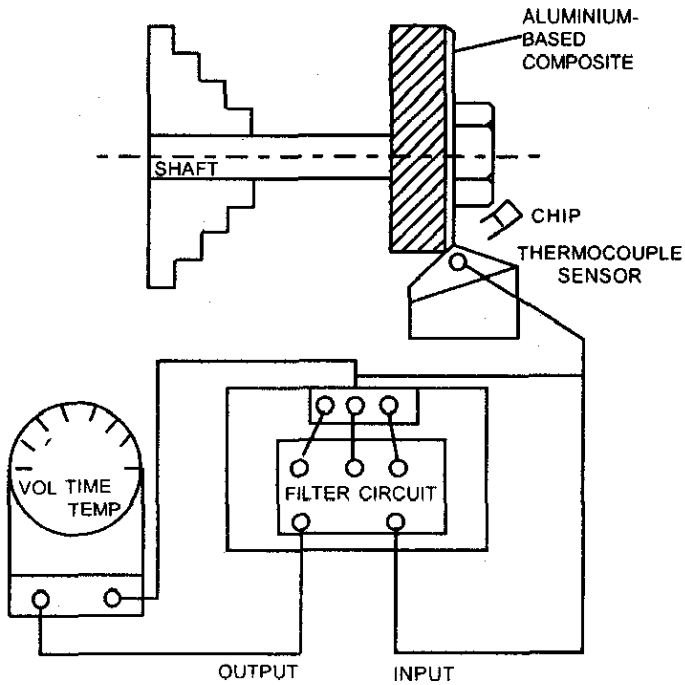

Figure 1. Thermocouple setup

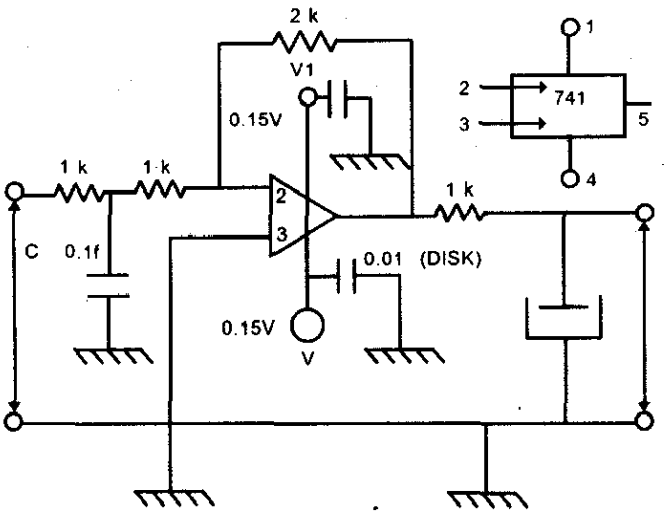

Figure 2. Filter circuit – (1) bread board, (2) 15-0-15 power supply, (3) digital millimeter, (4) 0-100 DC voltmeter.

was designed and used to amplify the obtained electromotive force values as these were too small to be detected by the voltmeter (multimeter). The thermocouple consisting of a sensor was placed at the chiptool junction and it served as the hot junction. The room temperature (i.e., the ambient temperature), was taken as the cold junction. The experiments were conducted for different cutting speeds, the depth of cuts (1 mm), feed rate constant (0.5 mm/rev) and the corresponding temperatures at the tool tip, middle of the tool, and the end of the tool were measured. Further, in the second experiment, temperature at the cutting edge was measured by varying speeds and depth of cuts while keeping the feed rate constant. The obtained values of electromotive force generated were converted to their corresponding temperatures after calibrating the thermocouple.

2.2 Calibration of Thermocouple

After conducting the turning experiment, it was necessary to calibrate the thermocouple to convert the obtained electromotive force values to their corresponding temperatures. The calibration was done using an electric muffle furnace. The tool tip and the workpiece were placed inside the furnace which served as the hot junction. The other end of the workpiece, outside the furnace, served as the cold junction. The electromotive force values were taken from the multitimer for a corresponding temperature thermocouple. The obtained temperatures for the same values of electromotive force during calibration were taken as the corresponding temperatures of the cutting tool during machining. The values of temperatures at different cutting speeds and at different points on the cutting tool, were obtained.

2.3 Problems in Machining of Composite Materials

The problems faced during machining of composite materials are numerous and differ from those of the conventional metals. It has been observed that a HSS tool fails within a few seconds while machining composite materials. The low thermal conductivity of a composite material causes heat build up in the cutting zones, which may also lead to thermal degradation of the matrix. These can be controlled using a coolant and also by machining at low feed rates. The use of a coolant depends on the properties of the workpiece material. Due to the cutting loads on the materials, high deflections occur, which may lead to delamination of the composite material. It has also been found that the fibres are abrasive, and due to this abrasive nature, rapid tool wear of the cutting tool occurs. This can be reduced using abrasive-resistant cutting tools like carbide tools. Also, due to enormous difference in the coefficient of thermal expansion between the fibre and the matrix, residual stresses are generated. This leads to difficulty in attaining dimensional accuracy. As seen, the chips are very small and are literally in the form of a powder. This hazardous, airborne dust may cause inconvenience while machining and can be removed by a dust extraction system.

3. RESULTS & DISCUSSION

3.1 Cutting Forces versus Cutting Speed

The cutting forces in MMCs are shown in Fig. 3. The cutting forces are reduced when the cutting speed is increased.

3.2 Wear Rate against Spindle Speed

The wear rate against the spindle speed is shown in Fig. 4. The primary wear is maximum

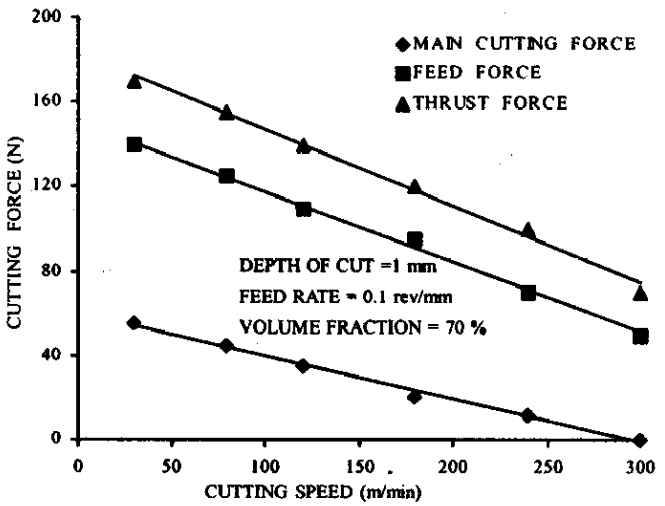

Figure 3. Variation of cutting forces against cutting speed

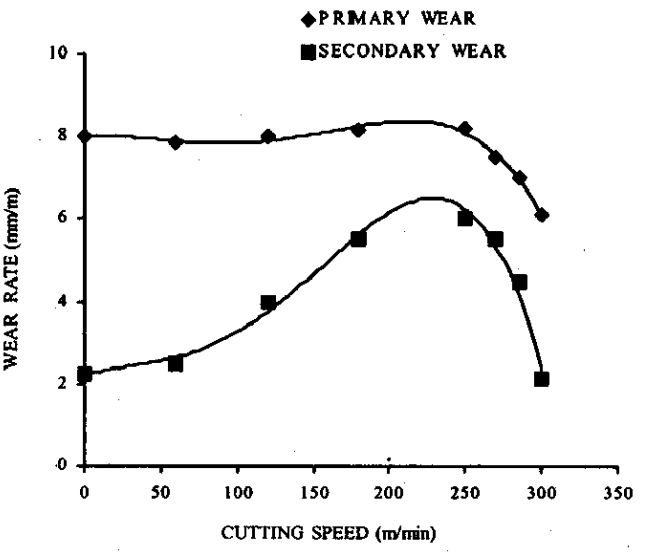

Figure 4. Variation of cutting speed against wear rate

at the cutting speed of 250 m/min and minimum at 300 m/min. The secondary wear is also the maximum at the cutting speed of 250 m/min and the least at 300 m/min. The cutting speed (i.e., 250 m/min) is the critical speed at which the groove wear rate and the nose wear rate are maximum. This is attributed to the failure of cutting edge as a result of softening of the tool material with an increase in the cutting temperature. This concludes that the critical speed is proportional to the hardness at room temperature (the hardness is proportional to the compressive strength). Hence, it is presumed that the compressive strength must play a significant role in an increase in the critical speed value, which shows the high speed cutting ability while machining of an MMC. In cutting relatively high thermal conductivity materials, the heat transfer from the cutting zone to the tool is resisted using a tool material with low thermal conductivity. The worn cutting edges observed from scanning electron microscope reveal roundish-banded wear in carbide tools, grooved wear, triangular wear in ceramites, and ceramic tools. Under critical speed, projector particles and gritty-worn surfaces are observed. The worn cutting edges observed from scanning electron microscope for HSS tool reveal that grooved wear exists heavily at the cutting edges.

3.3 Experimental Temperature Results

The temperature values have been experimentally found at different cutting speeds, (52 rpm, 88 rpm, 150 rpm, and 250 rpm) and are shown in Table 1. From Table 1, it can be observed that the temperatures show a gradual decrease as the distance from the cutting region increases. Moreover, it can also be seen that the temperature increases as the cutting speed increases, which comply with the general rules of metal cutting, since with an increase in the cutting speed, the cutting forces involved lead to more heat generation. Figure 5 shows the relationship between the depth of the cut and the cutting temperature at various cutting speeds. It can be seen from this figure that the temperature at the cutting edge is almost proportional to the depth of the cut. The

Table 1. Experimental temperature values at various cutting speeds

Cutting speed (rpm)	Location	Temp. (°C)
52	At the chip-tool interface	55
	At the midpoint of tool	54
	At the end of tool	51
88	At the chip-tool interface	65
	At the midpoint of tool	61
	At the end of tool	57
150	At the chip-tool interface	85
	At the midpoint of tool	80
	At the end of tool	75
250	At the chip-tool interface	105
	At the midpoint of tool	98
	At the end of the tool	95

number of contacts between the cutting edge and the thermocouple increase with an increase in the depth of the cut. Figure 6 shows linear variation of cutting forces against the cutting speeds when the feed rate and the depth of cut are constant. From this figure one can observe that the cutting forces gradually decrease when the cutting speed is increased.

4. FINITE-ELEMENT SOLUTION

The finite-element method is used to simulate the orthogonal machining. The tool is assumed to be stationary. The finite-element model of the cutting mechanism is shown in Fig. 7 The work tool and chip are treated as a single system in which, it is assumed, all the mechanical work is converted into heat. The governing differential equation for thermal conduction is given by

$$\kappa \{\partial^2 t/\partial x^2 + \partial^2 t/\partial y^2\} + q_h = 0 \qquad (1)$$

The main sources of heat generation in metal cutting are given by the shear zone (q_1), where the main plastic deformation occur; the chip tool interface zone (q_2), where secondary deformation due to friction between the chip and the tool takes place; and the work tool interface (q_3) at flank, where frictional rubbing occurs.

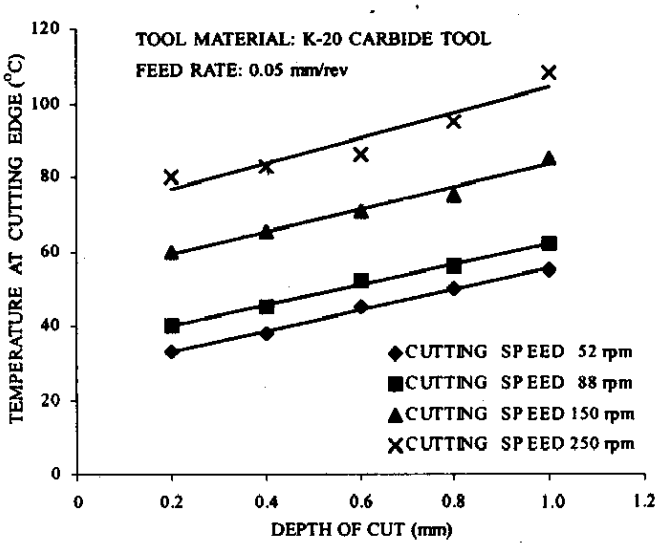

Figure 5. Variation of temperature at cutting edge against the depth of cut.

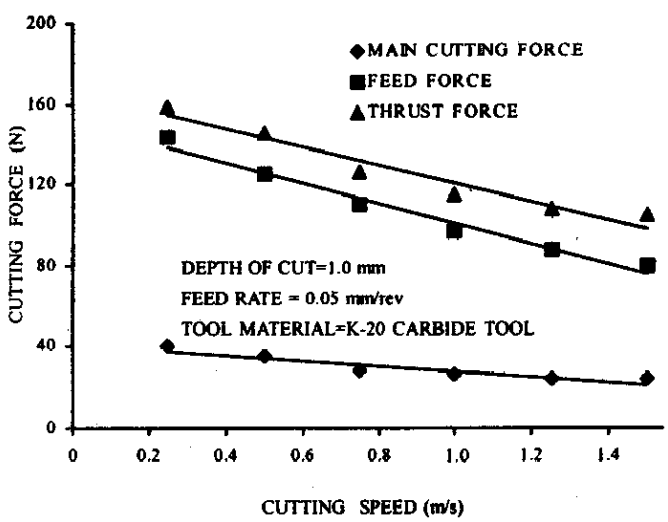

Figure 6. Variation of cutting forces against cutting speed

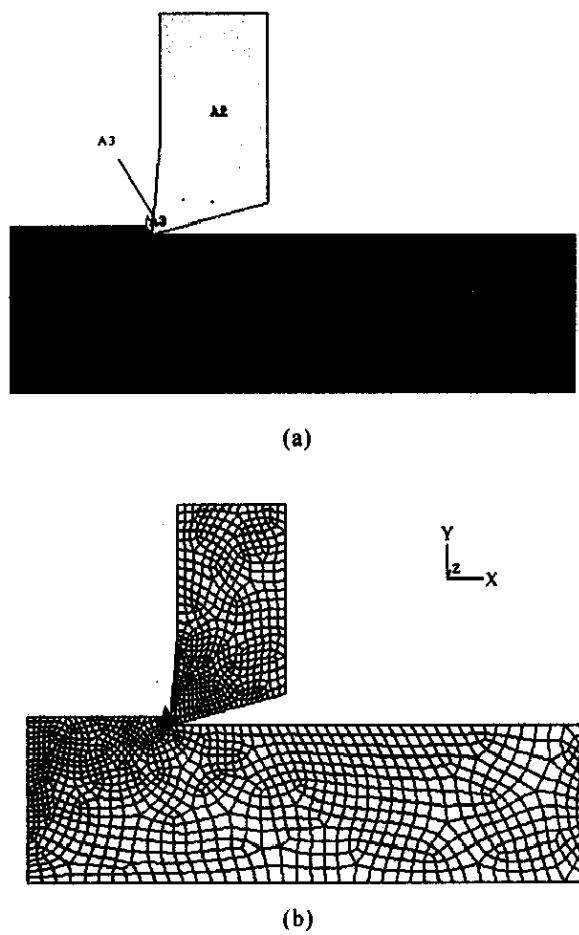

Figure 7. Geometry of orthogonal cutting mechanism along with finite-element model: (a) geometry of the work tool and chip of orthogonal cutting mechanism and (b) finite-element model (after convergence check).

4.1 Heat Generation in Metal Cutting

The heat generation rate in the primary plastic deformation zone per unit area is given by

$$q_1 = \frac{F_s V_s}{J ab \operatorname{cosec}\beta} \tag{2}$$

where

$$F_s = F_z \cos\theta - F_t \sin\theta$$

and

$$F_V = \frac{V_C \cos\delta_0}{\cos(\beta - \delta_0)}$$

From the analytical viewpoint, the friction between the chip and the tool can be regarded as a heat source that is moving in relation to the tool. The total frictional energy dissipated at the chip-tool interface for unit area is given by

$$q_2 = \frac{F V_f}{J b_1} \tag{3}$$

It is assumed that the sliding velocity over the flank wear land is constant and is equal to the work velocity. The heat flux over the flank wear land is constant and is given by

$$q_3 = \frac{0.0671\ F_Z V_C}{ab} \tag{4}$$

4.2 Finite-element Formulation

The temperature at any point is given by

$$T(x) = \sum_{i=1}^{n} N_i\ (x)\, T_i = NT \tag{5}$$

$$\frac{d}{dx} T(x) = \sum_{i=1}^{n} \frac{d}{dx} \{N_i(x) T_i\} = BT \tag{6}$$

The finite-element equation for heat conduction analysis is given by

$$[\kappa_C]\{T\} = \{q\} \tag{7}$$

where

$$[\kappa_C] = \int_V^T B\ KB\ \mathrm{d}v$$

and

$$\kappa = \begin{bmatrix} \kappa x x & 0 \\ 0 & \kappa y y \end{bmatrix}$$

$$q = \int_V^T N\ q^b\ \mathrm{d}v$$

4.3 Boundary Conditions

- The boundary of the workpiece is at room temperature because the boundary is quite far from the cutting region. Hence, there is no temperature gradient along this boundary, i.e., $dt/ds = 0$
- As the edge of the chip is nearer to the cutting region, so the specified temperature boundary conditions are imposed at the edge of the chip.
- The heat generation rates calculated (q_1, q_2, and q_3) are specified as boundary conditions.

4.4 Numerical Results

Figures 8 and 9 show the temperature variation in the cutting mechanism. Figure 8 shows the variation of the cutting temperature in the workpiece in radial direction against the cutting speed. From these figures it can be observed that the temperature is decreasing while one moves farthest from the cutting edge. Figures 9 and 10 show the variation of cutting temperature in axial direction, i.e., the tool flank contact surface. From these figures, it can be observed that the temperature is decreasing while one moves from the contact edge to farther away when increasing the cutting speed. The variation of cutting temperature in chip thickness

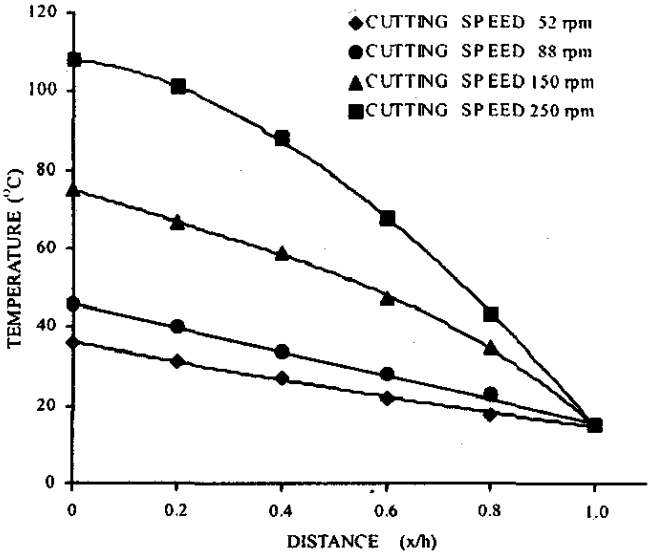

Figure 8. Variation of temperature against cutting speed (radial direction).

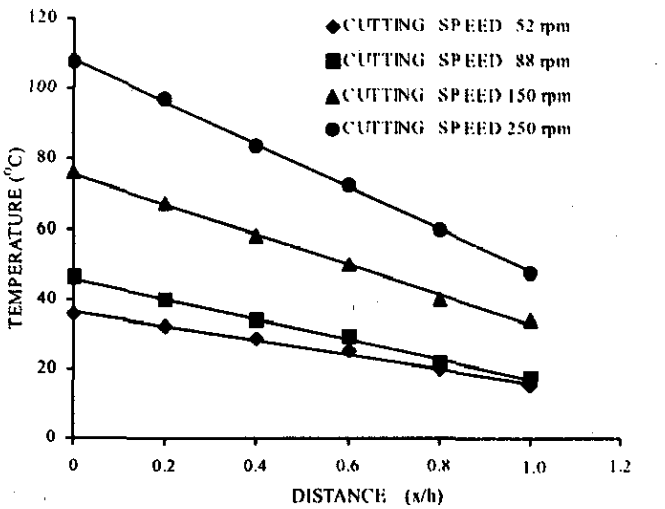

Figure 10. Variation of temperature against cutting speed (chip thickness).

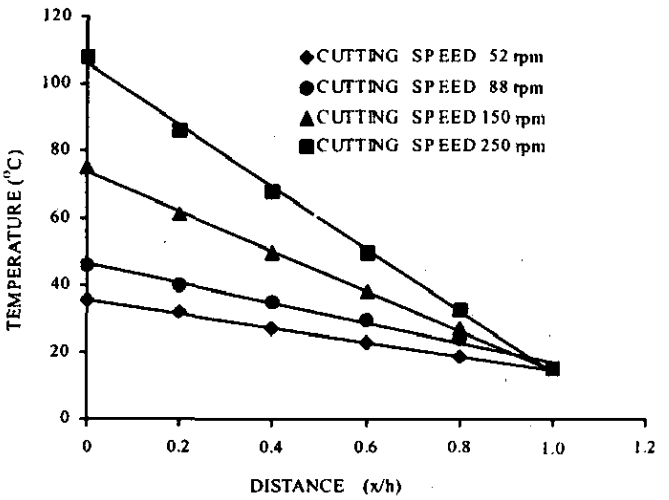

Figure 9. Variation of temperature against cutting speed (axial direction).

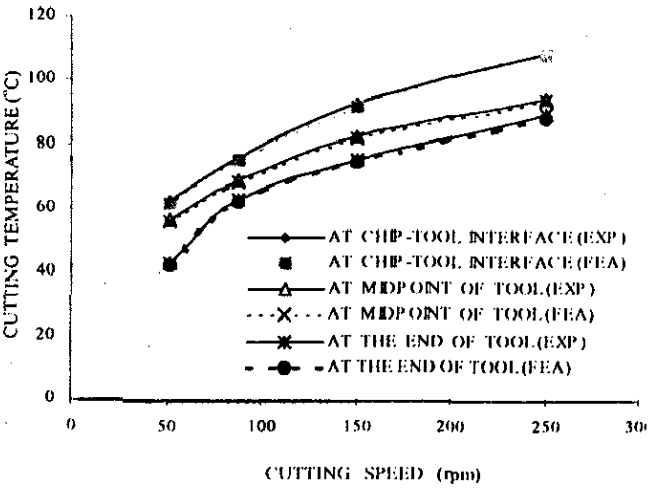

Figure 11. Variation of cutting temperature against cutting speed (both experimental and FEA results).

is shown in Fig. 10. The temperature at the chip-tool contact is very high and as one moves farther away from the contact, there is a gradual decrease in the temperature. From these figures, one can observe that most of the heat concentration is in the tool. This phenomenon is entirely different in metals, where most of the heat is carried away by the chip. The reason for this behaviour could be due to the difference in cutting mechanisms. In the composite materials, the cutting mechanism is more of brittle fracture, involving a combination of mechanisms like cutting, cracking, ploughing, and abrasion. Moreover, the very small contact length between the chip (dust or minute size of the chip) and the tool can also be explained as one of the reasons for the heat not been carried away by the chips. Figure 11 shows a comparative study of both the experimental and the finite element results of temperatures at various cutting speeds. From the graph, one can observe that the results show a good correlation between the two methods (variation of 1.25 per cent only).

ACKNOWLEDGEMENTS

The authors gratefully acknowledge the University Grants Commission for funding this research work.

REFERENCES

1. Lim, S.C. & Ashby, M.F. Overview-wear mechanism maps. *Acta Metallurgica*, 1985, **C35**, **N55**, 1-24.

2. Weight, P.K. Physical models of tool wear for adaptive control in flexible machining cells. *In* Proceedings of the Symposium on CIM, V8, ASME, 1986.

3. Kramer, B.M. & Suh, N.P. Tool wear by solution: A quantitative understanding. *J. Eng. Ind. Trans. ASME*, 1980, **102**, 303.

4. Bayoumi, A.E. & Kendall, L.A. Modelling and measurement of wear of coated and un-coated high speed steel end mills, *J. Mater. Shap. Technol.*, 1991.

5. Wu, S.M. Tool life testing by response surface methodology, Part I and II. *J. Eng. Ind. Trans. ASME*, 1964, **86**, 105.

6. Zdeblick, W.J. & Devot, R.E. An experimental strategy for designing tool life experiments. *J. Eng. Ind. Trans. ASME*, 1978, **100**, 441.

7. Machinability testing and utilization of machining data. *In* Proceedings of the International Conference of Machinability Testing and Utilization of Machining Data, American Society for Metals, September, 1978.

8. Evaluating machining performance of ferrous metals using an automatic screw/bar machine, E, 618. *In* Annual Book of ASTM Standards, American Society for Testing and Materials.

9. Influence of metallurgy on machinability. *In* Proceedings of the International Symposium, (Sponsored by the Machinability Activity of the Mechanical Working and Forming Division), American Society for Metals, October 1975.

10. Tool life testing with single-point turning tools. International Organization for Standardization, 1977. ISO–3685-1977.

11. Heginbotham, W.B. & Pandey, P.C. Taper turning tests produce reliable wear equations. *Adv. Mach. Tool Des. Res.*, 1966.

12. Thomas, J.L. & Lambert. B.K. Reliability of accelerated tool life testing method. Society of Manufacturing Engineerings, 1974. Technical Paper Mr 74-703.

13. Kiang, T.S. & Barrow, G. Determination of tool-life equations by step turning test. *In* International Machine Tool Design Research Conference Proceedings, September 1971. pp. 379-385.